Surfactant-free syntheses and pair distribution function analysis of osmium nanoparticles

Mikkel Juelsholt,[a,†] Jonathan Quinson,[a,†,*] Emil T. S. Kjær,[a] Baiyu Wang,[a] Rebecca Pittkowski,[a] Susan R. Cooper,[a] Tiffany. L. Kinnibrugh,[b] Søren B. Simonsen,[c] Luise Theil Kuhn,[c] María Escudero-Escribano[a] and Kirsten M. Ø. Jensen[a,*]

a. Department of Chemistry, University of Copenhagen, 5 Universitetsparken, 2100 Copenhagen, Denmark

b. X-ray Science Division, Advanced Photon Source, Argonne National Laboratory, Argonne, IL, USA

c. Department of Energy Conversion and Storage, Technical, University of Denmark, Fysikvej Bldg. 310, DK-2800 Kgs. Lyngby, Denmark

* Corresponding authors: jonathan.quinson@chem.ku.dk, kirsten@chem.ku.dk

† Equally contributing authors

Abstract

A surfactant-free synthesis of precious metal nanoparticles performed in low boiling point solvents and in alkaline conditions has been reported recently. This strategy presents several advantages over alternative colloidal syntheses. The resulting nanoparticles are readily relevant for applications like catalysis and the synthetic process is compatible with large scale production. Alkaline mono-alcohols are here investigated as solvent and reducing agents to obtain colloidal Os nanoparticles by this low temperature (< 100 °C) surfactant-free synthesis. The effect of precursor ($OsCl_3$ or H_2OsCl_6), precursor concentration (up to 100 mM), solvent (methanol or ethanol), presence or absence of base (NaOH) and addition of water (0 to 100 v.%) on the resulting nanomaterials is discussed. It is fond that no base is required to obtain Os nanoparticles as opposed to the case of Pt NPs for instance. The robustness of the synthesis for concentration of precursor up to 100 mM allows to perform X-ray total scattering with pair distribution function (PDF) analysis that shows that the 1-2 nm *hcp* NPs forms from chain-like $[OsO_xCl_y]$-complexes.

Introduction

Precious metals are limited resources yet fundamental for a range of key applications. Gold (Au), silver (Ag), platinum (Pt), palladium (Pd), ruthenium (Ru), rhodium (Rh) and iridium (Ir) for instance, are widely used and still explored in applications such as medicine, optics, chemical production, energy conversion, pollution management, to mention only a few.[1-3] Among the precious metals, osmium (Os) has been the focus of relatively few studies,[4] as illustrated in **Fig. S1**. The limited number of reports on Os is partly due to its scarcity and because Os easily forms highly toxic OsO_4 compounds. However, Os and Os-based complexes and nanomaterials have been reported[5-8] and studied for their catalytic, optical and medical properties,[9-15] in experimental and theoretical work.[16] For example, Os is expected to be an active catalyst for the energy relevant oxygen evolution reaction, though it suffers the drawback of poor stability.[17]

For precious metal nanomaterials to be applied in catalysis, higher activity is expected if the nanostructures expose a *clean* surface. However, common synthesis approaches require surfactants, viscous solvents or shape directing agents[15, 18-21] that act as ligands on the nanoparticle (NP) surface to stabilize the colloidal nanomaterials. These additives can bring impurities, can be toxic and add cost to the synthesis and so are detrimental to develop simpler and more sustainable syntheses of precious metal NPs. *Surfactant-free* syntheses therefore bear promising features for fundamental research but also industrial scale production.[22, 23] A surfactant-free synthesis method to produce Pt, Ir, Ru or bimetallic NPs has been reported recently.[22] It only requires a mono-alcohol as solvent and reducing agent,[24] a base and a metal precursor to obtain size controlled NPs.[25] This approach leads to catalysts that are more active than those prepared for example in polyols.[26, 27] A similar approach was successfully used to develop Pd NPs.[28] Here we investigate if this simple synthetic approach using mono-alcohols is suitable for the synthesis of Os NPs.

Studies of NP synthesis have made it clear that a number of seemingly simple experimental parameters can play a significant role for nanomaterial synthesis.[29] For example, it has recently been reported that Os NPs with an *hcp* structure were obtained using $OsCl_3$ precursor whereas *fcc* NPs were obtained with Os acetylacetonate.[19] We therefore here screen the influence of several experimental parameters across a large parametric space by investigating the influence of the precursor: $OsCl_3$ and H_2OsCl_6; the nature of solvent: methanol and ethanol; the absence or presence of a base (NaOH) and the effect of adding water: 0, 10, 25, 50, 66, 75 or 100 v.%. As opposed to the case of Pt, Ir, Ru or Pd, we observe that these experimental parameters have little influence on the resulting size and structure of the Os NPs. Small NPs of 1-2 nm are obtained and

structurally characterized using X-ray total scattering and pair distribution function (PDF) analysis, which also provides insight into the Os NP formation mechanism.

Experimental

Chemicals

$OsCl_3$ (Premion®, 99.99% metals basis), H_2OsCl_6 (Premion®, 99.95% metals basis), NaOH (98%, Alfa Aesar); methanol (≥99.9%, HiPerSolv Chromanorm®, VWR); ethanol (VWR, absolute, ≥ 99.5%); water (Milli-Q, Millipore, resistivity >18.2 MΩ·cm).

Os nanoparticle synthetic procedures

In a first approach and for a parametric study, the precursor for the Os nanomaterials were obtained from a 2.5 mM solution of $OsCl_3$ or H_2OsCl_6. The solvents used were methanol, ethanol or their mixture with water for different proportion of mono-alcohols and water indicated in v.% (before volume contraction). The syntheses were performed in the absence or presence of base (NaOH). The total volume of the precursor solution used was 2 mL, evaluated as the sum of the volume of water and alcohol before volume contraction. The mixtures were placed in sealed polypropylene tubes (15 mL centrifuge tubes, VWR, melting point of 160 °C) and placed in an oil bath, pre-heated at 90 °C, for 6 hours to obtain Os nanomaterials.

In a second approach for the purpose of X-ray scattering with PDF analysis, requiring a high concentration of scattering material, the samples were prepared in 3 mm NMR tubes (Wildmad®, 3 mm outer diameter, 0.27 mm wall thickness, Type 1 Class A) with a stirrer bar (Fisherbrand PTFE Stirrer bar, 8x1.5 mm). Here, the precursor concentration was 100 mM ($OsCl_3$ or H_2OsCl_6), and the samples were prepared in 0.2 mL methanol or ethanol and water mixture in volume ratio alcohol:water of 1:2. Identical samples, but without $OsCl_3$ or H_2OsCl_6 were used for background measurements. The samples (with and without metal precursor) were left to react at 85 °C for several hours for *in situ* measurements or for a week (with precursor) under stirring, as indicated.

Characterisation

Transmission electron microscopy (TEM). Few drops of the as prepared nanomaterials were dropped on TEM grids (Ni, Quantifoil) prior to imaging with a Jeol 2100 transmission electron microscope. For each sample, images were recorded in a least three randomly selected areas at least at three different magnifications. The NPs size was estimated by measuring the diameter of at least 100 NPs using the ImageJ software.

X-ray diffraction (XRD). X-ray powder diffraction was measured on a Bruker D8 diffractometer with a Cu anode equipped with a Ni filter in Bragg-Brentano geometry. The samples were prepared by drop-casting a suspension of the NPs onto a Si-111 zero background sample holder. Data from each sample were measured from 5-80° 2θ.

Small angle X-ray scattering (SAXS). SAXS characterization protocols and samples preparation are detailed in the Supplementary information (SI).

Pair distribution function (PDF) analysis. Total scattering measurements were performed at beamline 11-ID-B at the Advanced Photon Source, Argonne National Laboratory. The samples were loaded into NMR tubes with a 3 mm diameter and 0.27 mm thickness and placed in dedicated holders. The data were collected with a wavelength of λ = 0.2113 Å using a 2D PerkinElmer detector with a pixel size of 200x200 μm in the rapid acquisition pair distribution function setup.[30] The detector distances were calibrated from a CeO_2 standard in Fit2D[31] and the 2D images were integrated using Dioptas.[32] Background subtraction and Fourier transform into the pair distribution function (PDF) were done using xPDFsuite with a Qmax of 21 $Å^{-1}$ for the samples containing precursors and 23.8 $Å^{-1}$ for samples containing the Os NPs.[33] The obtained PDFs were analyzed using PDFgui[34] and Diffpy-CMI.[35] The metallic cluster models were generated using the ASE package.[36]
The fitting procedure of the Os NPs was performed by generating a large number of different Os clusters, including simple cubic, *fcc*, *bcc* and *hcp*, as well as icosahedra, octahedra, decahedra and Wulff constructions with different combinations of surfaces and potentials.[36] Each cluster was fitted to the data by refining a scale factor, a single atomic displacement parameter for all the atoms and a correlated motion parameter, δ_2. Furthermore, a lattice for each cluster was also refined, which allows the cluster to expand and contract isotropically.[37] Fits using crystalline models were done by refining the scale factor, lattice parameters, a single atomic displacement parameter for all the atoms and a correlated motion parameter, δ_2. The effects of the NP size were either modelled using a single spherical particle size or a lognormal distribution of spherical particles as implemented in Diffpy-CMI.

Results and discussion

Parametric study

The synthesis of Os NPs is here easily performed in closed containers made of polypropylene as described in the experimental section. As opposed to a classical reflux set up using glassware,[22] or to the use of microwaves,[38] visible or UV light,[39] this allows for a rapid screening of a number of experimental parameters for long synthesis times, e.g. 6 hours at moderate temperature, e.g. 90 °C. **Table S1** gives an overview of the different parameters investigated for this parametric study. **Figs. S2-S18** gather TEM micrographs of the materials synthesized.

Influence of solvent composition. In absence of alcohol, i.e. when using water as solvent, no or few NPs were observed on the TEM grid. This suggests the need for methanol or ethanol to play the role of reducing agent to obtain Os nanomaterials.

Influence of water content. Adding water is a useful approach to increase the size of Pt NPs in alkaline mono-alcohol syntheses,[25] although this approach is not effective for size-control for Ir NPs.[39] For the Os synthesis, we also see no effect on the size of the Os NPs of the water content when evaluating NP size with TEM. However, adding water leads to the formation of network-like structures reported in **Figs. S2-18**, although the exact nature of this network is not yet established. The networks formed in the presence of water are not observed in the synthesis of Pt, Ir or Ru NPs.[22, 25, 27] The focus is here on obtaining Os NPs.

Role of the base. A range of precious metal NP colloidal syntheses are reported to be successful only under alkaline conditions and the amount of base can be used to control the NPs size, e.g. in the polyol synthesis.[40, 41] For Pt and Ir NP syntheses, the reaction does not proceed in absence of a base in methanol or ethanol, unless performed at elevated temperatures/pressure or supercritical conditions.[42] However, in the case of Os synthesis, individual NPs are obtained at relatively low base concentration, as seen in **Fig. S18**, and more remarkably even in the absence of a base, **Figs. S20-21**. This is also shown in **Fig. 1** displaying TEM micrographs of the NPs obtained for different precursors and solvents. Again, we see no clear effect of base concentration on particle size. The Os NPs forming are in all cases ca. 1-2 nm.

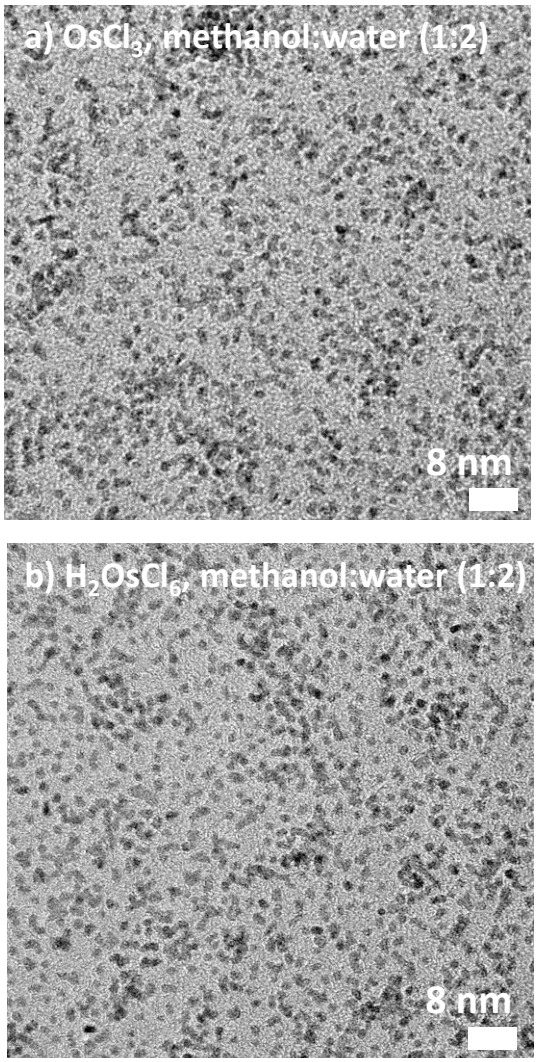

Fig. 1. (a-d) TEM micrographs of Os NPs obtained using 66 v.% water and 33 v.% methanol (no base) and 100 mM (a) $OsCl_3$ and (b) H_2OsCl_6 as precursor after 1 week reaction at 85 °C in NMR tubes (volume ca. 0.2 mL). The size analysis suggest that the NPs are (a) 1.6 ± 0.4 nm, (b) 1.7 ± 0.3 nm.

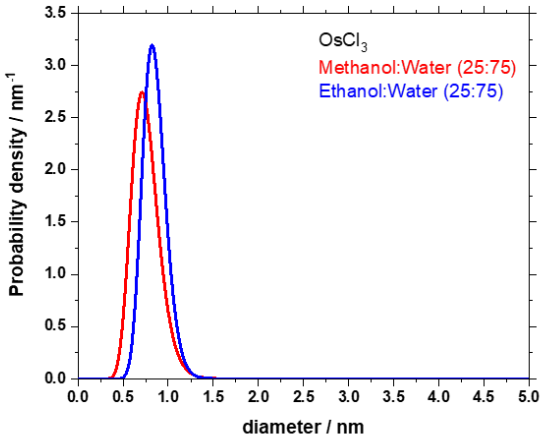

Fig 2. Probability densities retrieved from the SAXS analysis of the Os NP size. The sample displayed were obtained with 2.5 mM $OsCl_3$ in absence of base for a methanol:water mixture of 1:35 in volume after 6 hours at 90 °C for a total volume of 2 mL.

Influence of the mono-alcohol. We have previously shown that in the synthesis of Pt NPs, the solvent plays a key role incontrolling the synthesis mechanism and the resulting diameter of the NPs.[24] For Os, the NPs are around 1-2 nm in diameter and the particle size appears independent of the nature of the solvent, as confirmed by SAXS analysis, see **Fig. 2, Fig. S22** and **Table S2**. Although methanol is more toxic than ethanol, it is a simpler molecule less prone to side reactions. It is therefore considered a more suitable solvent in the context of fundamental research studies.[24, 43]

Optimal synthesis parameters. The size of the Os NPs is also not significantly influenced by the type of precursor used, $OsCl_3$ or H_2OsCl_6. The less hydrophilic $OsCl_3$ precursor was considered a simpler precursor to use. The amount of water used in the synthesis has also little influence on the resulting NP size. To develop a simple and relatively cheap synthesis requiring only few chemicals, it was concluded that $OsCl_3$, no base and relatively high water content around 60-75 v.% using methanol as reducing agent were favourable conditions to obtain Os NPs for further studies.

PDF characterisation

In line with the small size of the NPs obtained here in the range 1-2 nm, see for example **Fig. 1** and **Fig. S23**, most reported colloidal synthesis methods of Os NPs yield nanomaterials in the size range 1-2 nm. This can further explain why the interest for Os NPs has been limited to date: the small size limits the material characterization that can be done with conventionally available methods. Relatively high-resolution transmission electron microscopy (TEM) is needed to characterize small nanomaterials,[15, 19, 44, 45] and X-ray diffraction (XRD) analysis is challenged due to the broadening of Bragg peaks for ca. 1-

2 nm NPs. Due to the very small NP size, XRD analysis of the Os samples actually shows no identifiable Bragg peaks, **Fig. S24**.

We therefore turned to X-ray total scattering and pair distribution function analysis (PDF) to analyse the atomic structure of the Os NPs.[43] Since these experiments require high concentrations of materials when data are collected from samples in solution, a slightly different synthetic approach was used to prepare the different samples. The NPs were synthesized in a 3 mm NMR tube with 100 mM of precursor in mono-alcohol:water volume ratio of 1:2 for a total volume of ca. 200 µL. The solutions were left at 85 °C in the closed NMR tubes for 1 week. The sealed NMR tubes were shipped from Copenhagen, Denmark to 11-ID-B beamline of the Advanced Photon Source (APS) at Argonne National Lab, USA, for measurements. TEM confirms the formation of 1-2 nm NPs, see **Fig. 1** and **Fig S23**, i.e. the materials are comparable to those obtained in the syntheses done in larger volumes and lower Os concentrations, see **Fig S2-S18**.

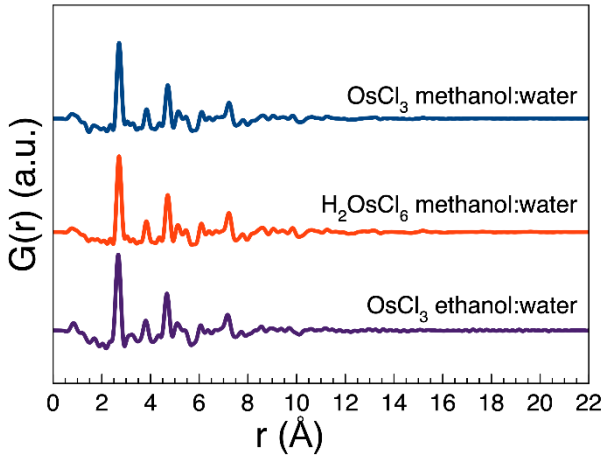

Fig. 3. PDFs obtained from 4 different synthesis of Os NPs in 1:2 alcohol:water ratios and for different precursors as indicated. The PDFs can be described using a *hcp* model.

Total scattering data and PDFs were obtained from NPs synthesised from $OsCl_3$ and H_2OsCl_6 in a methanol:water mixture and $OsCl_3$ in an ethanol:water mixture. The total scattering signal is shown in **Fig. S25** and the resulting PDFs in **Fig. 3**. The PDFs of the 3 samples are more or less identical, which is in line with the parameter study that these parameters do not influence the formed NPs. From the extent of features in the PDFs, it can be concluded that the NPs are all smaller than 2 nm with an average crystallite size between 1 and 2 nm which is in agreement with TEM and SAXS characterisation as discussed above.

On the nanoscale, metallic NPs are known to be able to take different structures that those of bulk metals, and icosahedral or decahedral motifs are often observed for metals with normally closed-packed structures.[46] By using the atomic simulation environment (ASE) module[36] and the cluster-mining approach developed by Banerejee et al.[46] we screened a large number of metal NP clusters, including *hcp*, *fcc* and *bcc*, but also structures such as icosahedrons and decahedrons.

The synthesised Os NPs are best described using a small *hcp* cluster as seen in **Fig. 4** and **Figs. S26-31**, which agrees with the bulk *hcp* Os structure. The cluster that best fit the PDF obtained for NPs formed in methanol:water from H_2OsCl_6 contains 96 Os atoms. The clusters formed from $OsCl_3$ appear slightly smaller, with the best fitting structure for the particles formed in methanol:water containing 72 atoms, and those formed in ethanol:water containing 64 atoms. The largest cluster used for the refinement is *ca.* 13.5x8.2x6.5 $Å^3$ along the hexagonal crystallographic axes. The intermediate clusters are around 13.5x5.5x6.5 $Å^3$ and the smallest cluster is 8.1x8.1x6.5 $Å^3$. Several *hcp* clusters 0.3-0.6 Å larger in different directions provided fits of almost the same quality which indicates a distributed size of the NPs which is consistent with the SAXS and TEM data. Examples of fits using other types of clusters are seen in **Figs. S28-31**.

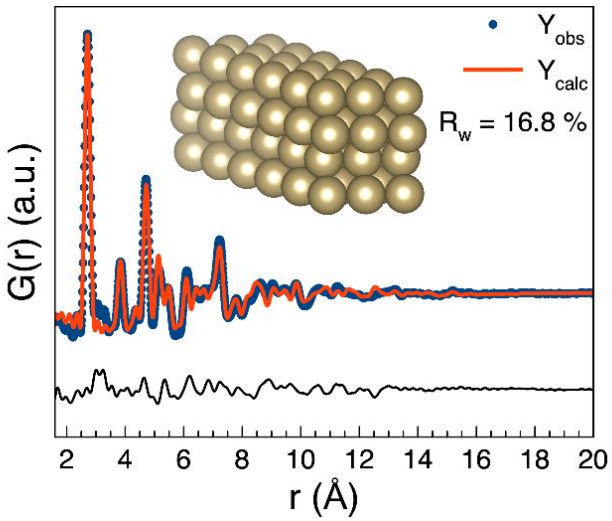

Fig. 4. Fit of a *hcp* cluster (seen in the insert) to the PDF obtained from the Os NPs formed in methanol:water from $OsCl_3$.

The sizes of the clusters used for the refinement should not be taken as absolute sizes of the NPs themselves, but instead describe any anisotropy induced from the *hcp* structure on the NP shape. To verify the validity of the cluster models, we also fitted the PDFs with spherical NPs with a single particle diameter and a lognormal size distribution, and those

fits are seen in **Figs. S32-S38**. For the smallest NPs, formed from $OsCl_3$ in ethanol:water, all models give a fit of the same quality, which is reasonable as the cluster model identified (8.1x8.1x6.5 $Å^3$) is almost isotropic. However, for the largest NPs, formed from H_2OsCl_6 in methanol:water, the discrete, anisotropic cluster model provides a better fit than that from a spherical particle model. This illustrates that for an accurate description of the atomic structure of small NPs it is important to consider any possible anisotropy induced by the crystal structure.

As seen in **Fig. S39** the PDFs from the Os NPs synthesised from $OsCl_3$ in ethanol:water show a small peak corresponding to an interatomic distance at 3.2 Å. A small indication of the same peak may be seen as a shoulder for the two samples synthesized in methanol. The distance is not described in the *hcp* model. We considered if this peak could originate from a ligand binding to the surface of the NPs, however, 3.2 Å is significantly longer than Os-O, Os-C and Os-Cl bond distances which are ca. 1.8 Å, 1.9 Å and 2.3 Å, respectively. However, this peak at 3.2 Å could correspond to an Os-Os distance in a $[Os_2Cl_2]$ complex which may be present in the solution, as discussed further in the SI.

A PDF from NPs synthesised from H_2OsCl_6 in ethanol:water was also obtained and is shown in **Fig. S40** As discussed in details in the SI, this PDF shows that the NPs synthesised from H_2OsCl_6 in ethanol:water have oxidised and so while the NPs remain mainly non-oxidised in solution they can oxidise over time or upon drying to form OsO_4.

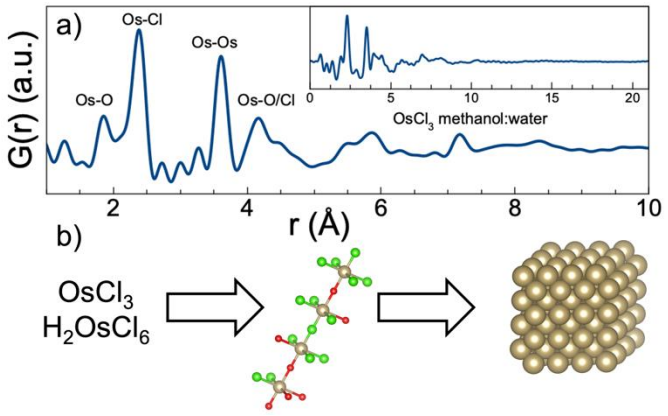

Fig. 5. a) Measured PDF of $OsCl_3$ in methanol:water. The insert shows the same PDF plotted to 21 Å. b) Overall formation mechanism of the *hcp* Os NPs. The Os chloride precursor reacts with the alcohol:water mixture to form chain-like structures of. $[OsO_xCl_y]$-octahedra which after long incubation time forms Os NPs. Os, Cl and O atoms shown in grey, green and red, respectively.

Precursor structure

Total scattering experiments on the precursor solution were also performed, see **Figs. 5** and **S41-45**. The resulting PDFs, are very similar to the PDFs of crystalline OsOCl compounds, e.g. $OsOCl_2$ and $(NH_4)_4(OsOCl_{10})$, which form chain-like structures. Both structures are shown in **Figs. S43** and **S44**. This indicates that the precursors react with the solvent and form a network of chain-like structures of $[OsO_yCl_x]$-octahedra, as illustrated in **Fig. 5**. The network is quite stable and even after 6 hours at 85 °C, minimal changes in the PDF occur for this high concentration of precursor (100 mM) syntheses, see **Fig. S46**. This stresses the need for longer syntheses time to initiate the breakdown of the precursor at high precursor concentration. This observation is in line with recent report on a formation mechanism involving chain-like structure made for the synthesis of Pt NPs.[43]

Conclusions

Os NPs with a *hcp* crystal structure and a size around 1-2 nm are synthesized in methanol and ethanol and water mixtures from $OsCl_3$ or H_2OsCl_6 precursors, without the need for surfactants. As opposed to the synthesis of Pt, Ir, Ru or Pd NPs by a similar approach, no base is here required. A synthesis using methanol:water in the volume ratio (1:2) with $OsCl_3$ as precursor was here considered optimal. The results presented show that size control of Os NPs is a challenging task and even at high precursor concentration up to 100 mM small size 1-2 nm in diameter NPs are obtained. X-ray total scattering measurement with PDF analysis show that the samples take the *hcp* structure, and it is shown that the Os NPs from from $[OsO_xCl_y]$-complexes.

This study and the versatile synthesis introduced provide a suitable platform to inspire future study of the formation mechanism of Os based nanomaterials and explore their properties further.

Author Contributions

Conceptualization: JQ KMØJ; Data curation: MJ, JQ, ETSK; Funding acquisition: KMØJ; Formal analysis: MJ, JQ; Investigation: MJ, JQ, ETSK, BW, RB, SRC, TLK; Project administration: JQ, KMØJ; Resources: SBS, LTK, MEE; Supervision: JQ, KMØJ; Visualisation: MJ, JQ; Writing - original draft: MJ, JQ; Writing - review and editing: MJ, JQ, ETSK, BW, RB, SRC, TLK, SBS, LTK, MEE, KMØJ.

Conflicts of interest

There are no conflicts to declare.

Acknowledgements

KMØJ is grateful to the Villum Foundation for financial support through a Villum Young Investigator grant (VKR00015416). This work was supported by the Danish National Research Foundation (DNRF-149) Center for High-Entropy Alloys Catalysis (CHEAC). J. J. K Kirkensgaard and the Niels Bohr institute, University of Copenhagen, are thanked for access to SAXS. This research used resources of the Advanced Photon Source, a U.S. Department of Energy (DOE) Office of Science User Facility, operated for the DOE Office of Science by Argonne National Laboratory under Contract No. DE-AC02-06CH11357 (GUP-72059).

References

1. M. Azharuddin, G. H. Zhu, D. Das, E. Ozgur, L. Uzun, A. P. F. Turner and H. K. Patra, *Chem. Commun.*, 2019, **55**, 6964-6996.
2. P. Losch, W. X. Huang, E. D. Goodman, C. J. Wrasman, A. Holm, A. R. Riscoe, J. A. Schwalbe and M. Cargnello, *Nano Today*, 2019, **24**, 15-47.
3. I. Chakraborty and T. Pradeep, *Chem. Rev.*, 2017, **117**, 8208-8271.
4. J. Hamalainen, T. Sajavaara, E. Puukilainen, M. Ritala and M. Leskela, *Chem.Mater.*, 2012, **24**, 55-60.
5. R. D. Adams and Z. W. Luo, *J. Organomet. Chem.*, 2016, **812**, 108-114.
6. L. Han, P. F. Wang, H. Liu, Q. Q. Tan and J. Yang, *J. Mater. Chem. A*, 2016, **4**, 18354-18365.
7. J. Kraemer, E. Redel, R. Thomann and C. Janiak, *Organometallics*, 2008, **27**, 1976-1978.
8. A. Pitto-Barry, K. Geraki, M. D. Horbury, V. G. Stavros, J. F. W. Mosselmans, R. I. Walton, P. J. Sadler and N. P. E. Barry, *Chem. Commun.*, 2017, **53**, 12898-12901.
9. S. Anantharaj, U. Nithiyanantham, S. R. Ede and S. Kundu, *Ind. Eng. Chem. Res.*, 2014, **53**, 19228-19238.
10. O. Metin, N. A. Alp, S. Akbayrak, A. Bicer, M. S. Gultekin, S. Ozkar and U. Bozkaya, *Green Chem.*, 2012, **14**, 1488-1492.
11. A. Egeberg, C. Dietrich, C. Kind, R. Popescu, D. Gerthsen, S. Behrens and C. Feldmann, *ChemCatChem*, 2017, **9**, 3534-3543.
12. C. S. Lim, Z. Sofer, R. J. Toh, A. Y. S. Eng, J. Luxa and M. Pumera, *ChemPhysChem*, 2015, **16**, 1898-1905.
13. C. Sanchez-Cano, D. Gianolio, I. Romero-Canelon, R. Tucoulou and P. J. Sadler, *Chem. Commun.*, 2019, **55**, 7065-7068.
14. A. T. Odularu, P. A. Ajibade, J. Z. Mbese and O. O. Oyedeji, *J. Chem.*, 2019, **2019**.

15. S. B. He, L. Yang, P. Balasubramanian, S. J. Li, H. P. Peng, Y. Kuang, H. H. Deng and W. Chen, *J. Mater. Chem. A*, 2020, **8**, 25226-25234.
16. M. C. S. Escano, R. L. Arevalo, E. Gyenge and H. Kasai, *Catal. Sci. Technol.*, 2014, **4**, 1301-1312.
17. N. Danilovic, R. Subbaraman, K.-C. Chang, S. H. Chang, Y. J. Kang, J. Snyder, A. P. Paulikas, D. Strmcnik, Y.-T. Kim, D. Myers, V. R. Stamenkovic and N. M. Markovic, *J. Phys. Chem. Lett.*, 2014, **5**, 2474-2478.
18. Z. Q. Niu and Y. D. Li, *Chem. Mater.*, 2014, **26**, 72-83.
19. T. Wakisaka, K. Kusada, T. Yamamoto, T. Toriyama, S. Matsumura, G. Ibrahima, O. Seo, J. Kim, S. Hiroi, O. Sakata, S. Kawaguchi, Y. Kubota and H. Kitagawa, *Chem. Commun.*, 2020, **56**, 372-374.
20. U. Nithiyanantham, S. R. Ede and S. Kundu, *J. Mater. Chem. C*, 2014, **2**, 3782-3794.
21. C. Vollmer, E. Redel, K. Abu-Shandi, R. Thomann, H. Manyar, C. Hardacre and C. Janiak, *Chem. Eur. J.*, 2010, **16**, 3849-3858.
22. J. Quinson, S. Neumann, T. Wannmacher, L. Kacenauskaite, M. Inaba, J. Bucher, F. Bizzotto, S. B. Simonsen, L. T. Kuhn, D. Bujak, A. Zana, M. Arenz and S. Kunz, *Angew. Chem. Int. Ed.*, 2018, **57**, 12338-12341.
23. J. Quinson, S. Kunz and M. Arenz, *ChemCatChem*, 2021, **13**, 1692-1705.
24. J. Quinson, S. Neumann, L. Kacenauskaite, J. Bucher, J. J. K. Kirkensgaard, S. B. Simonsen, L. T. Kuhn, A. Zana, T. Vosch, M. Oezaslan, S. Kunz and M. Arenz, *Chem. Eur. J*, 2020, **26**, 9012-9023.
25. J. Quinson, L. Kacenauskaite, J. Bucher, S. B. Simonsen, L. T. Kuhn, M. Oezaslan, S. Kunz and M. Arenz, *ChemSusChem*, 2019, **12**, 1229-1239.
26. F. Bizzotto, J. Quinson, J. Schröder, A. Zana and M. Arenz, *J. Catal.*, 2021, **401**, 54-62.
27. F. Bizzotto, J. Quinson, A. Zana, J. J. K. Kirkensaard, A. Dworzak, M. Oezaslan and M. Arenz, *Catal. Sci. Technol.*, 2019, **9**, 6345-6356.
28. J. Quinson, S. B. Simonsen, L. T. Kuhn, S. Kunz and M. Arenz, *RSC Adv.*, 2018, **8**, 33794-33797.
29. J. Quinson and K. M. Ø. Jensen, *Adv. Colloid Interface Sci.*, 2020, **286**, 102300.
30. P. J. Chupas, X. Qiu, J. C. Hanson, P. L. Lee, C. P. Grey and S. J. L. Billinge, *J. Appl. Crystallogr.*, 2003, **36**, 1342-1347.
31. A. Hammersley, *J. Appl. Crystallogr.*, 2016, **49**, 646-652.
32. C. Prescher and V. B. Prakapenka, *High Press Res.*, 2015, **35**, 223-230.
33. X. J. Yang, Pavol; Farrow, Christopher L.; Billinge, Simon J. L., 2014. arXiv:1402.3163v3. https://arxiv.org/abs/1402.3163
34. C. L. Farrow, P. Juhas, J. W. Liu, D. Bryndin, E. S. Božin, J. Bloch, P. Th and S. J. L. Billinge, *J. Phys.: Condens. Matter*, 2007, **19**, 335219.

35. P. Juhas, C. L. Farrow, X. Yang, K. R. Knox and S. J. L. Billinge, *Acta Cryst. A*, 2015, **71**, 562-568.
36. A. Hjorth Larsen, J. Jørgen Mortensen, J. Blomqvist, I. E. Castelli, R. Christensen, M. Dułak, J. Friis, M. N. Groves, B. Hammer, C. Hargus, E. D. Hermes, P. C. Jennings, P. Bjerre Jensen, J. Kermode, J. R. Kitchin, E. Leonhard Kolsbjerg, J. Kubal, K. Kaasbjerg, S. Lysgaard, J. Bergmann Maronsson, T. Maxson, T. Olsen, L. Pastewka, A. Peterson, C. Rostgaard, J. Schiøtz, O. Schütt, M. Strange, K. S. Thygesen, T. Vegge, L. Vilhelmsen, M. Walter, Z. Zeng and K. W. Jacobsen, *J. Phys.: Condens. Matter.*, 2017, **29**, 273002.
37. K. M. O. Jensen, P. Juhas, M. A. Tofanelli, C. L. Heinecke, G. Vaughan, C. J. Ackerson and S. J. L. Billinge, *Nat. Commun.*, 2016, **7**, 11859.
38. J. Quinson, J. Bucher, S. B. Simonsen, L. T. Kuhn, S. Kunz and M. Arenz, *ACS Sustain. Chem. Eng.*, 2019, **7**, 13680-13686.
39. J. Quinson, L. Kacenauskaite, J. Schroder, S. B. Simonsen, L. T. Kuhn, T. Vosch and M. Arenz, *Nanoscale Adv.*, 2020, **2**, 2288-2292.
40. Y. Wang, J. W. Ren, K. Deng, L. L. Gui and Y. Q. Tang, *Chem. Mater.*, 2000, **12**, 1622-1627.
41. J. Quinson, M. Inaba, S. Neumann, A. A. Swane, J. Bucher, S. B. Simonsen, L. T. Kuhn, J. J. K. Kirkensgaard, K. M. O. Jensen, M. Oezaslan, S. Kunz and M. Arenz, *ACS Catal.*, 2018, **8**, 6627-6635.
42. D. Saha, E. D. Bojesen, K. M. O. Jensen, A. C. Dippel and B. B. Iversen, *J. Phys. Chem. C*, 2015, **119**, 13357-13362.
43. J. K. Mathiesen, J. Quinson, A. Dworzak, T. Vosch, M. Juelsholt, E. T. S. Kjaer, J. Schroder, J. J. K. Kirkensgaard, M. Oezaslan, M. Arenz and K. M. O. Jensen, *J. Phys. Chem. Lett.*, 2021, **12**, 3224-3231.
44. Y. Wang, J. L. Zhang, X. D. Wang, J. W. Ren, B. J. Zuo and Y. Q. Tang, *Top. Catal.*, 2005, **35**, 35-41.
45. H. Hirai, Y. Nakao and N. Toshima, *J. Macromol. Sci. Chem.*, 1979, **A13**, 727-750.
46. S. Banerjee, C.-H. Liu, K. M. O. Jensen, P. Juhas, J. D. Lee, M. Tofanelli, C. J. Ackerson, C. B. Murray and S. J. L. Billinge, *Acta Cryst. A*, 2020, **76**, 24-31.